Waves, Mean Flows, and Mixing at a Seamount

Charles C. Eriksen

School of Oceanography, University of Washington, Box 357940, Seattle WA 98195-7940

Abstract. Moored array measurements of current and temperature at Fieberling Guyot (32° 25'N, 127° 47'W) are dominated by internal wave and tidal band fluctuations. Internal wave band variance on the flanks of the seamount is dominated by amplification of waves by reflection at and near the local critical frequency of the sloping bottom. Diurnal, slightly superinertial, and semidiurnal band fluctuations exhibit coherent downward phase propagation. These have the character of a forced evanescent response as opposed to free vertically-radially standing seamount trapped wave modes. At depths near the summit rim, mean horizontal flows have a component toward deeper water, while on the flanks mean flows are much weaker but have a component toward shallower water. In both cases, the mean Eulerian flows appear driven by fluctuations.

Introduction

Until recently, very little was known about the character of oceanic flow near seamounts, particularly seamounts that occupy a substantial fraction of the water column. Most observations and theories were concerned with distortions of mean flows by isolated topographic features rather than with wavelike fluctuations found near them. Theories have addressed the possibility that Taylor caps may isolate water above a seamount from surrounding water masses. Chapman and Haidvogel, 1992, considered formation of Taylor caps over large seamounts, in contrast to much previous work restricted to considering topography that occupied only a small fraction of the total depth. By contrast, observations at Fieberling Guyot, a large seamount in the eastern North Pacific (32° 25'N, 127° 47'W) show that flows are dominated by fluctuations rather than the mean. These fluctuations are predominately tidal (Eriksen, 1991, Brink, 1995) in the depth range bracketing the summit and centered at the critical frequency for internal wave reflection off a slope deep on the seamount flanks (Eriksen, 1995). Mean flows are generally parallel to depth contours near the bottom in an anticyclonic sense but do have slight cross-isobath components. Near the summit, horizontal flows are in the off-slope sense, consistent with local downwelling (Eriksen, 1991, Brink, 1995), yet on the steep flanks of the seamount, flows near the bottom have an onslope (radially inward) sense. This paper discusses the possibility that these radial mean flows are associated with the fluctuating flows in tidal and internal wave bands.

The paper begins with a brief summary of the structure of internal wave band motions on the steep flank of Fieberling Guyot and their connection to mixing events. The description and analysis of Eriksen, 1995, is extended to include buoyancy and momentum flux estimates and their spatial structures. The following section presents a description of motions in diurnal and semidiurnal frequencies and the band between them, which includes the inertial frequency. Brink, 1995, confined his description to motions in tidal bands near the seamount summit, while motions over a continuum across the inertial frequency all exhibit a similar structure, including continuous downward phase propagation to the bottom on the sloping flanks. As with internal waves, these motions generate eddy fluxes of buoyancy and momentum. Kunze, 1995, recognized the phase structure of flow atop Fieberling in velocity profile surveys and showed the consistency in several respects of a vortex trapped internal wave model with these observations, in contrast to Brink's seamount trapped wave model. Here, we offer another possible explanation: that the motions observed are an evanescent wave response to forcing across a wide range of frequencies, both subinertial and superinertial. Finally, the paper examines the mean flows observed both near the summit and on the flank of the seamount, emphasizing the radial component of flow near the bottom from which vertical motion is inferred. In the last section, the possibility that internal wave breaking and evanescent wave rectification generates mean flows is discussed.

The Field Study

The observations used here were collected as part of a multi-disciplinary project called TOPO, sponsored by the U.S. Office of Naval Research. The field program at Fieberling Guyot included a thirteen-month moored array of current and temperature sensors at various locations on and near the seamount. Details of the records are presented in Wichman *et al*, 1993. Records considered here are from moorings were set near the summit (C), at

the rim of the summit plain (R2 and R3), and on the seamount flanks (F2, F3, F4, and F5) (Figure 1). These moorings were located over one quadrant rather than on all sides of the guyot for reasons of economy. Seamount bathymetry was surveyed with a multi-beam depth sounder prior to the deployment cruise and again, in more detail near the mooring sites, on the recovery cruise. The cluster consisting of three moorings F3, F4, and F5, each separated by roughly 300 m on the southwest flank of the seamount, formed an internal wave array while the summit, rim, and flank moorings together formed an array to detect bottom-trapped motions that propagate azimuthally around the seamount.

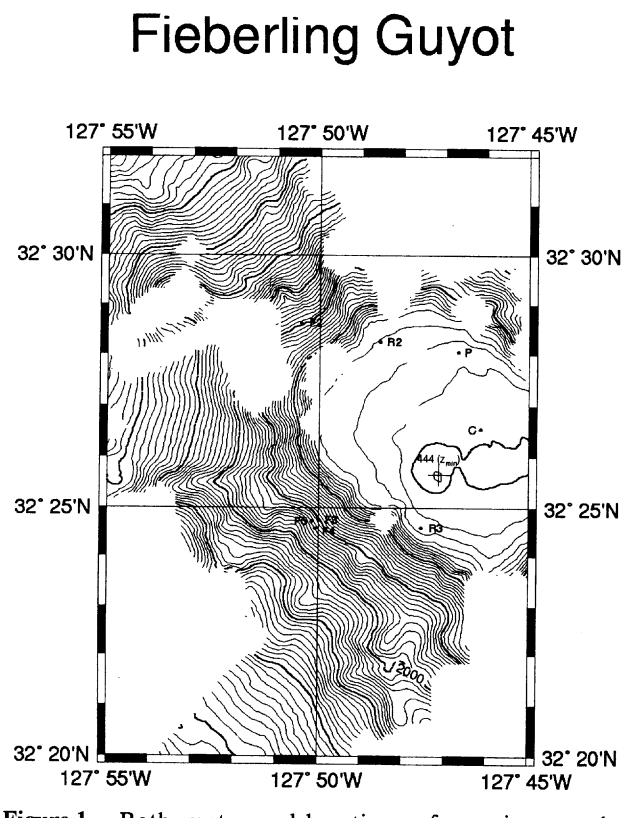

Figure 1. Bathymetry and locations of moorings on the western summit region of Fieberling Guyot. The moorings designated C, R, and F were placed near the center, on the rim of the summit plain, and on the flanks of the seamount. The triangle of moorings F3, F4, and F5 formed an internal wave array. The mooring P was from a pilot study one year before the rest of the array was set (see Eriksen, 1991). Depth contours are from a partial Hydrosweep survey of the seamount on the mooring recovery cruise on *R/V Thompson*. Depth contours are drawn every 50 m with every tenth contour drawn with heavy curve. The summit, a rocky spur is at 444 m depth. The seamount rises from a surrounding region of 4500 m depth.

Roden, 1991, 1994, allowed use of his conductivity-temperature-depth (CTD) surveys near Fieberling Guyot in August, 1989 and May, 1991 to calculate average temperature and salinity profiles, temperature-salinity relationships, and buoyancy frequency profiles. These are used to interpret temperature fluctuations variously as buoyancy or vertical velocity fluctuations through assuming that temperature fluctuations are reflect vertical advection of the mean gradient field.

Standard techniques of spectral analysis were applied to a common 364-day period subset of the records starting October 1, 1990. Independent spectral estimates were formed by averaging over 13 adjacent frequency bands for periods 12 h and longer and doubling the amount of averaging for each successive octave above the semidiurnal band. Complex empirical orthogonal functions (CEOFs) are used to describe the coherent structures of variability in each frequency band. This technique uses the eigenvalues and eigenvectors of a cross-spectral matrix (or coherence matrix) to describe variability in terms of the independent coherent structures ranked by their contribution to the total variance (Wallace and Dickinson, 1972, Eriksen, 1985). Consideration is limited to frequency bands in which a single empirical mode dominates. This has the effect of eliminating incoherent fluctuations from calculations of eddy fluxes and their gradients.

Internal Wave Structure

Internal wave band fluctuations on the flank of Fieberling Guyot are dominated by the process of wave reflection from a sloping boundary. While linear theory for the ideal case of reflection off an infinite sloping plane is consistent with several aspects of this process, nonlinearities are clearly apparent as well (Eriksen, 1995). Internal waves incident on a sloping boundary are obliged to change their wavenumber magnitude upon reflection. For downward rays incident from deeper water, reflection magnifies the vertical and onslope components of wavenumber. This magnification is forced by the requirement to match the projection parallel to the slope of incident and reflected wavenumbers. Waves incident at arbitrary orientations to the sloping boundary are turned more normal to isobaths by reflection. The energy density of reflected waves is amplified over that of incident waves by the ratio of the vertical wavenumber amplification squared because both ray tube widths and group speeds are inversely proportional to the vertical wavenumber amplification. Reflected waves dominate the wave field due to energy density enhancement and the enhancement is greater nearer the internal wave critical frequency σ_c where incident rays match the bottom slope.

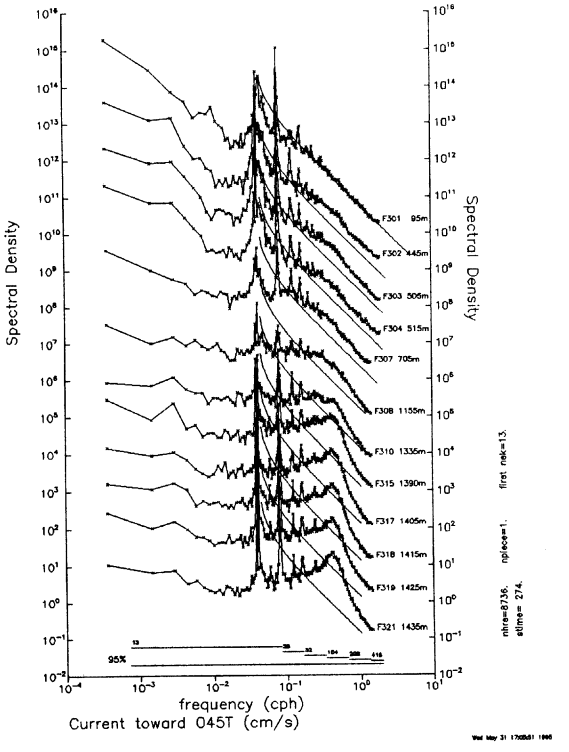

Figure 2. Spectra of the onslope (northeast) component of current on mooring F3 on Fieberling Guyot. Spectra are labeled by instrument number and depth and are arranged in order of depth from 95 m to 1435 m (where the anchor depth of the mooring was 1455 m). Scales are correct for the deepest spectral estimate (F321) and are successively offset by one decade for spectra at shallower depths. Smooth curves superimposed are the Garrett-Munk model estimates for the open deep ocean and serve as references fro the observed spectra. Their endpoints are at the inertial frequency f and the local buoyancy frequency N. Spectra are enhanced about the internal wave critical frequency σ_c = 0.42 cph. Intervals of 95% confidence are based on frequency averaging of a multiple of 13 independent spectral estimates.

The spectra of current in the onslope direction (i.e. normal to local isobaths) calculated from the records on F3, the heavily instrumented mooring in the internal wave cluster on the southwest flank of the seamount, indicate substantial departure from the Garrett-Munk model spectra that characterize deep open ocean spectra (Figure 2). The departure is strongest near the bottom and takes the form an enhancement at the local critical frequency σ_c = 0.42 cph. The enhancement around the critical frequency is evident even several hundred m above the bottom, while the spectrum from 95 m depth closely matches the Garrett-Munk prediction. A single CEOF describes half or more of the variance in each frequency band in the bottom 300m, from an octave below to an octave above the critical frequency (Eriksen, 1995). When records from all depths on mooring F3 are decomposed into CEOFs, two frequency ranges stand out as being dominated by a single mode: a band from 24 through 16 h and a band from about 4 to 1.5 h (Figure 3). Discussion of the longer period band motions is deferred until below. The shorter period band is centered on the local internal wave critical frequency.

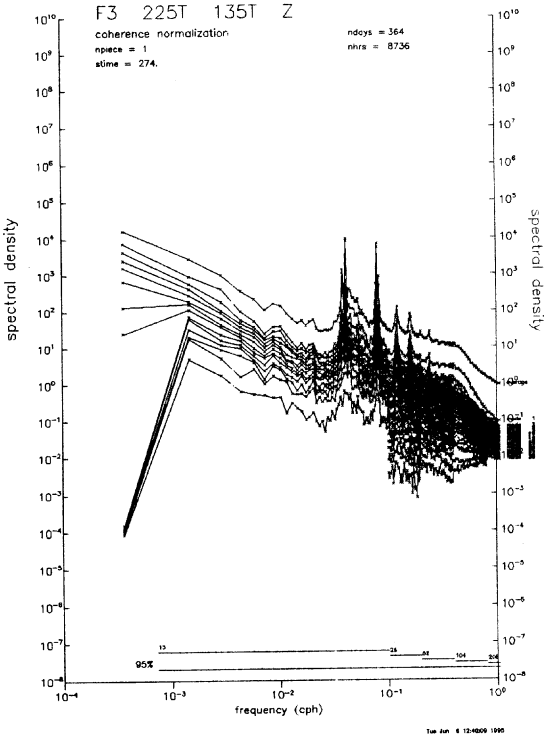

Figure 3. Spectra of complex empirical orthogonal functions calculated from the eigenvalues and eigenfunctions of the coherence matrix of current and temperature records on mooring F3. The top curve gives the average spectrum and each curve below it depicts the energy density accounted for by successively higher empirical mode. A single CEOF dominates structure over a band from the diurnal peak to a period of roughly 16 h and also over a band from about 4 to 1.5 h period, as is evident in the distinct separation of the second curve from the top from all other curves below it over these ranges.

Both spectra and the complex eigenfunctions that dominate variance near the critical frequency indicate that linear theory accounts for much of the behavior of motions in the internal wave band. Linear features include the transition between prominent upward and

offslope phase propagation at subcritical frequencies to downward and onslope propagation at supercritical frequencies. Waves are aligned across isobaths near the critical frequency, as expected by the linear theory of internal wave reflection off a sloping bottom. Linear theory is also consistent with the observed ratio of vertical to horizontal wavenumber for these eigenfunctions.

Linear theory fails to account for the finite enhancement of spectra at the critical frequency itself, for the decay of spectral enhancement with height off the bottom, and the vanishing of wavenumber at the critical frequency rather than the presence of only very fine scales. Statically unstable conditions are frequently found in the bottom few hundred m on the seamount flank. More than 11% of Richardson number estimates over a 10 m separation are found to be negative while altogether more than 25% are less than 0.25. Shear and density gradient fluctuations near the critical frequency dominate variance in the internal wave band as well as overall variance. Internal wave reflection is responsible for wave breaking, hence loss from the wave field to dissipation and to production of potential energy (buoyancy mixing). The rate of potential energy production diminishes with distance from the bottom, suggesting a convergence of turbulent fluxes.

Records from the internal wave array can be used to compute eddy fluxes of heat and momentum. Since the temperature-salinity relationship is well defined in the depth range of instruments on moorings F4 and F5 and those nearby on F3, temperature can reliably be converted to density to form fluctuation buoyancy b' where $b' \equiv -g\,(\rho - \bar{\rho})\,\rho_0^{-1}$ is the departure from the mean with ρ signifying density, g density, mean quantities have an overbar, and reference values have a subscript zero. Since vertical velocity is not measured directly, a vertical advection assumption $b'_t + N^2 w' = 0$ is used, where N is the average buoyancy frequency. The possibility of estimating vertical eddy transport of buoyancy is, of course, precluded.

The structure of eddy fluxes calculated from the dominant complex eigenfunction structure integrated across the internal wave band shows an offslope buoyancy transport that diminishes with distance from the sloping bottom (Figure 4, top left panel). Accompanying this flux are onslope and upward fluxes of momentum. These two results can be traced to the rotation in time of current vectors in the vertical plane normal to isobaths: their sense is to turn clockwise when viewed with shallow water on the right (Eriksen, 1995). The convergence of these fluxes suggests mean Eulerian flows, as discussed below.

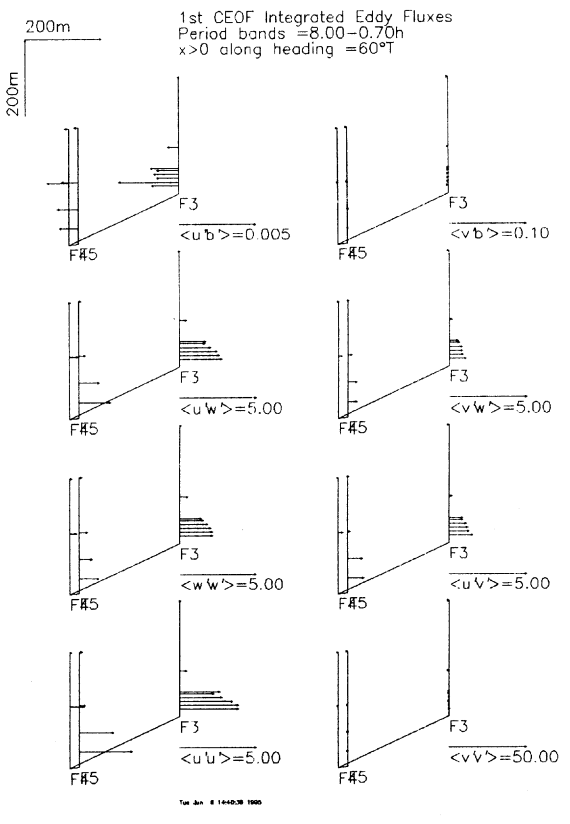

Figure 4. Internal wave band eddy fluxes of momentum (lower six panels) and buoyancy (top two panels) calculated from the first CEOF describing variability within 300 m of the bottom at moorings F3, F4, and F5. Fluxes are drawn as vectors in the vertical plane along 60°T heading (the local onslope direction). Perturbation current components are taken as a right-handed triad with u in the onslope direction. Units given in the scale are cm^2/s^2 for momentum and cm^2/s^3 for buoyancy fluxes.

Diurnal through Semidiurnal Structure

A single empirical mode dominates flow structure in the diurnal and semidiurnal tidal frequency bands, but also over a broad range of periods from diurnal (subinertial) to about 16 h (superinertial). The dominant mode has similar, but not identical, structure throughout this range. CEOF spectra illustrate the dominance of a single empirical mode at the tidal peaks O_1, P_1-K_1 (the latter are indistinguishable in a one year record), M_2, and S_2 (Figure 3). They also illustrate the less pronounced, but still evident, dominance of a single mode from slightly subinertial (0.94f) to somewhat superinertial (1.46f) frequencies (where f = 1/22.385 cph is the inertial

frequency. The inertial frequency divides this range dynamically, since free internal gravity waves are possible only at superinertial frequencies. Despite this division, coherent bottom-trapped flow patterns of similar structure are found over a broad range of frequencies spanning it.

The existence of a roughly cylindrically symmetric first azimuthal mode diurnal oscillation trapped near the summit at Fieberling Guyot has recently been documented. Brink, 1995, gives an interpretation in terms of radially and vertically standing free modes whereas Kunze, 1995, noted the predominance of downward propagating phase in the clockwise component of current, consistent with the pilot mooring results (Eriksen, 1991). Similar flow structures appear over a broad range of frequencies, not simply at the diurnal tidal lines. Moreover, downward propagating phase is a consistent feature of these oscillations.

Above the seamount summit and near the summit rim, currents are nearly circularly polarized in the clockwise sense both at the diurnal tidal frequencies and across the continuum from diurnal to a frequency 50% above diurnal. The higher the frequency in this band, the more eccentric the current ellipse. By contrast, currents near the bottom on the flank of the seamount are nearly rectilinearly polarized with flow nearly parallel to the local isobaths. Current component and vertical displacement amplitudes tend to be highest at depths between those of the summit and the summit plain rim (Figure 5), even when scaled in a WKBJ sense by the local stratification, with the exception that amplitudes tend to rise sharply at the bottom. (Following the stretching convention of Kunze, 1995, the reference buoyancy frequency is 3 cph and depths are stretched from the ocean surface; the seamount summit (444 m) is at 570 stretched m and the summit plain rim (700 m) is at 750 stretched m.) The total range of amplitudes is rather small, only a factor of two or so.

The CEOF decomposition describes the temporal relationship between measured quantities through their relative phases. Current component and displacement phases all tend to increase with depth (Figure 6) indicating downward phase propagation. The rates of change of phase are different for the different flow components because their relative phases differ with position. For example, offslope (southwestward) current lags alongslope (southeastward) current by roughly 90° near the summit but is nearly in phase with it at depth, hence phase change rates with depth are different for the two components. The rate of phase increase with depth for the azimuthal component of flow gives a stretched vertical wavenumber of about 1 cycle per stretched vertical km downward at 24 h period. At 16 h period, the

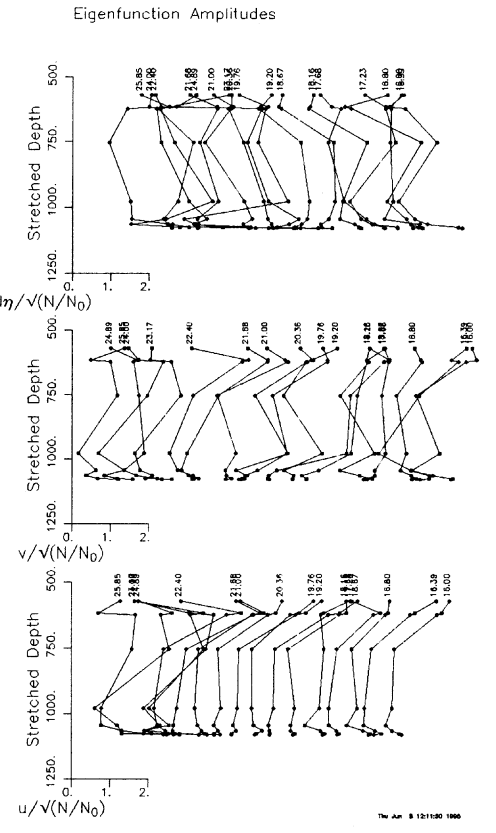

Figure 5. WKBJ scaled current and vertical displacement eigenfunction amplitudes for the first CEOF mode on mooring F3. The three panels give scaled amplitudes for the offslope component u (bottom panel), the alongslope component in the anticlockwise direction around the seamount v (middle panel), and upward displacement times buoyancy frequency $N\eta$ (top panel). Depth is stretched by the local buoyancy frequency with a reference N_0 = 3 cph. The upper three estimates are from depths near the summit, the fourth is from just below the summit rim, and the five deepest estimates are from near the bottom along the seamount flank. Independent frequency estimates, labelled by period in h, are successively offset by 0.5 in amplitude.

wavenumber magnitude is reduced to about 2/3 cycle per stretched vertical km.

The amplitudes and relative phase between offslope (equivalent to radial in cylindrical geometry) current and vertical displacement determine the contribution to eddy buoyancy flux from each frequency band. Kunze, 1995, notes that eddy buoyancy flux from diurnal period oscillations is in the offslope direction. The CEOF formalism allows eddy fluxes to be calculated from the coherent fluctuations of current and temperature across the moored array. We use records from the three moorings C, R3, and F3 to describe the onslope-vertical

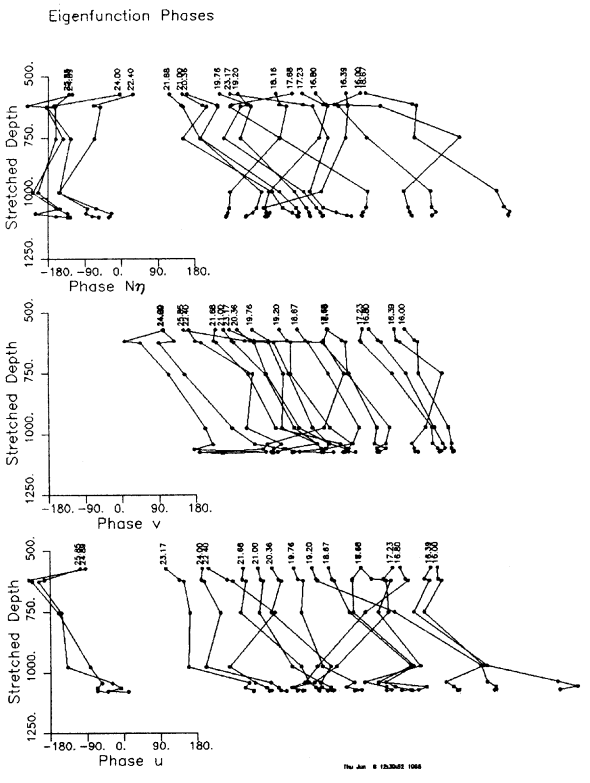

Figure 6. First CEOF mode current and vertical displacement eigenfunction phases on mooring F3 plotted against WKBJ stretched depth as in Figure 5. The three panels give relative phases for the offslope component u (bottom panel), the alongslope component in the anticlockwise direction around the seamount v (middle panel), and upward displacement times buoyancy frequency $N\eta$ (top panel). Phases have been adjusted by integral cycles to minimize implied wavenumber magnitude. Independent frequency estimates, labelled by period in h, are successively offset by 45° in phase. The phase convention is that more positive phases lag.

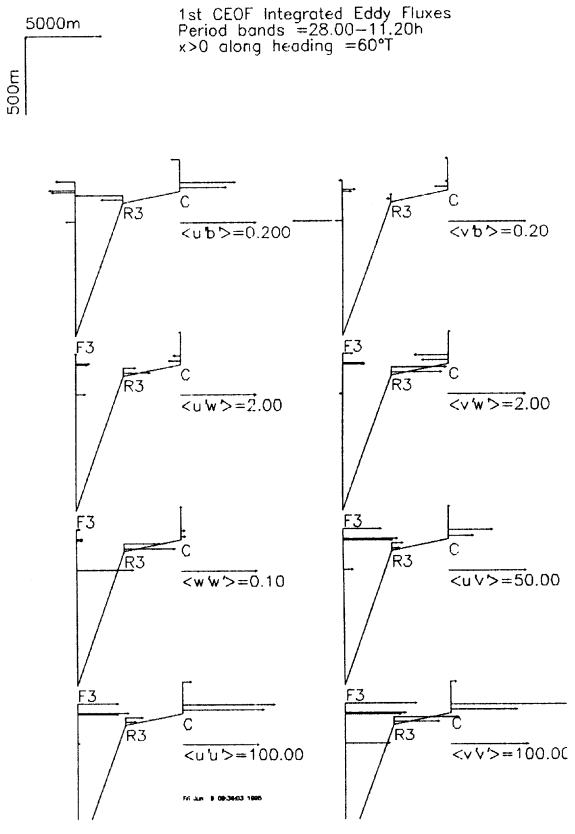

Figure 7. Diurnal through semidiurnal band eddy fluxes of momentum (lower six panels) and buoyancy (top two panels) calculated from the first CEOF describing variability at depths in a range about the summit depth at Fieberling Guyot using moorings C, R3, and F3. Fluxes are drawn as vectors in the vertical plane along 60°T heading (the local onslope direction). Perturbation current components are taken as a right-handed triad with u' in the onslope direction. Units given in the scale are cm^2/s^2 for momentum and cm^2/s^3 for buoyancy fluxes.

structure of eddy fluxes (Figure 7). The onslope gradient of onslope buoyancy flux contributed by tidal and intertidal frequency oscillations (an integration from 28 to 11.2 h periods, top left panel, Figure 7) changes sign from offslope in the region over the summit plain to onslope in the region over the seamount flank (over a depth range encompassing the summit). Likewise, there is a sign change in the onslope gradient of onslope eddy transport of azimuthal momentum $\langle u'v' \rangle$ between the summit plain and the seamount flank as well. The vertical eddy flux of azimuthal momentum $\langle v'w' \rangle$ has the same vertical gradient above both the summit plain and the flank. The gradients of these eddy fluxes can be related to mean Eulerian flows through the equations for azimuthally and temporally averaged flow, expressed in cylindrical coordinates:

$$UU_r + WU_z - \frac{V^2}{r} - fV - P_r = -\frac{1}{r}\langle ru'^2 \rangle_r - \langle u'w' \rangle_z + \frac{\langle v'^2 \rangle}{r} \quad (1)$$

$$UV_r + WV_z + \frac{UV}{r} + fU = -\langle u'v' \rangle_r - \langle w'v' \rangle_z \quad (2)$$

$$UW_r + WW_z - P_z = -\frac{1}{r}\langle ru'w' \rangle_r + \langle w'^2 \rangle_z \quad (3)$$

$$WN^2 = -\frac{1}{r}\langle ru'b'\rangle_r - \langle w'b'\rangle_z \quad (4)$$

where (r,θ,z) and (u,v,w) are the offslope, alongslope, and vertical coordinates and velocity components, upper case quantities designate means, primed quantities indicate fluctuations, brackets denote averages, subscripts denote derivatives, N is buoyancy frequency, f the Coriolis parameter, and P is pressure. In the limit of weak mean flows, the nonlinear terms on the left sides of (1) through (3) can be neglected in favor of the balances $U = f^{-1}(-\langle u'v'\rangle_r - \langle w'v'\rangle_z)$ (from (2)) and (4) to give a mean onslope-vertical circulation. Noninteraction theorems (McIntyre,1980) caution that such an Eulerian circulation is exactly compensated by an opposite Stokes drift in the case that the fluctuations take the form of steady, inviscid, unforced waves. Nevertheless, current meters sense Eulerian flow, hence the spatial structures of coherent buoyancy and momentum fluxes indicated in Figures 4 and 7 may be expected to produce flow in the offslope-vertical plane. Estimates of these wave-induced flows are compared with measured mean flows in the following section.

Mean Flows

One year mean flows measured by current meters near the bottom on Fieberling Guyot tend to have an offslope component over the summit plain (at sites C, R2, and R3; see Brink, 1995) and onslope component over the flanks (at sites F2 and F3). Mean currents farther from the bottom tend to be more parallel to isobaths, although the orientation of bottom contours is depth dependent due to departures of the topography from perfect radial symmetry.

Currents at site R2 on the northwest side of the seamount (Figure 8) show the mean anticyclonic circulation above the summit region as a flow most intense about 105 m above the bottom (535 m depth). The current spiral turns leftward with depth at this site and current within the strongest part of the anticyclone appears to be parallel to the bottom contours. Flow closer to the bottom is offslope at roughly 1 cm/s while flow above the anticyclone maximum appears onslope at about the same rate. Mean current at site R3, also on the summit plain rim, is similarly sheared, with an offslope component near the bottom of about 1 cm/s as a departure from otherwise alongslope flow in the anticyclonic sense around the seamount (Figure 9). The mean flow 50 m off the bottom (535 m depth) is 10.3 cm/s in contrast to 12.4 cm/s found at the same depth, but a greater distance from the geometric center of the seamount, at site R2.

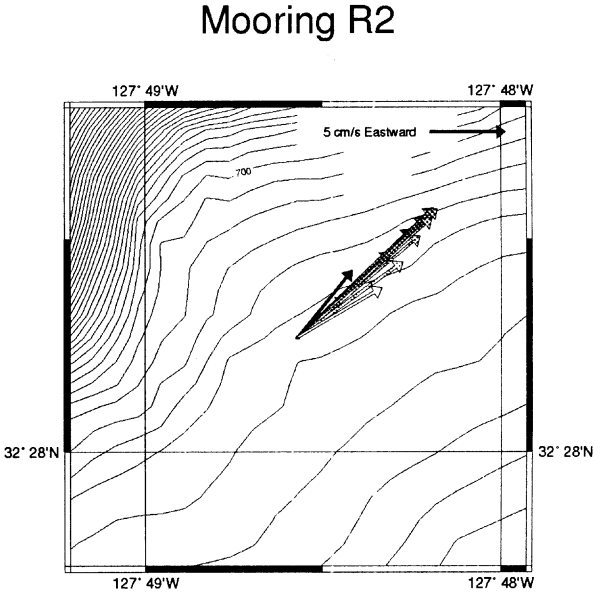

Figure 8. Mean flow over one year starting October 1, 1990, at 15, 35, 55, 75, 95, 115, 135, 155, 175, and 195 m above the bottom at the ADCP mooring site R2. Vectors are shaded in order of depth (the closest to bottom is solid). Depth contours at 10 m intervals are based on a Hydrosweep survey and the mooring position is based on acoustic and undithered GPS navigation. (Surveyed depth exceeds that inferred from the moored pressure record by 6 m at this site.)

Mean current on the flanks of the seamount is weaker and is directed slightly in the onslope direction, in contrast to the flow near the summit plain rim (Figure 10). Records from various locations within the internal wave array on the southwest flank have onslope flow components of up to about 0.2 cm/s. None of the currents measured within 160 m of the bottom over one year indicates an offslope component of flow. Moreover, the observed current vectors suggest an onslope component of flow even when compared to nearby isobaths of corresponding depth. Progressive vector diagrams (not shown) indicate that onslope flow exists even when the alongslope current is in the opposite sense for a few days or more.

Alongslope currents near the bottom tend to be modulated with a fortnightly signal in phase with the diurnal tidal current amplitude, although they vary also with low frequency flow impinging on the seamount (Eriksen, 1991, Brink, 1995, Kunze, 1995). That is, when diurnal fluctuations are strong, the anticyclone atop Fieberling is strong and conversely. This suggests that circulation near the seamount is, at least in part, due to rectification of tidal fluctuations. The onslope component may also be influenced by fluctuations, diurnal and

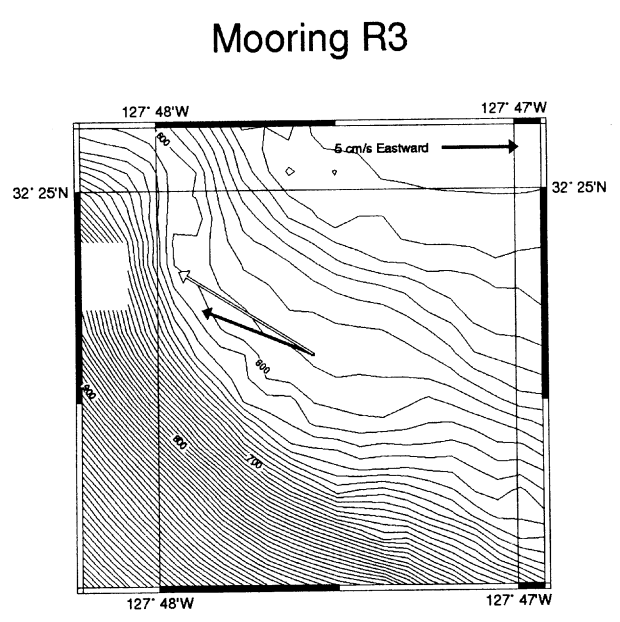

Figure 9. Mean flow over one year starting October 1, 1990, at 20 and 50 m above the bottom at the mooring site R2. The deeper vector is solid. Depth contours at 10 m intervals are based on a Hydrosweep survey and the mooring position is based on acoustic and undithered GPS navigation. Surveyed depth exceeds that inferred from moored pressure records by 3 m at this site.

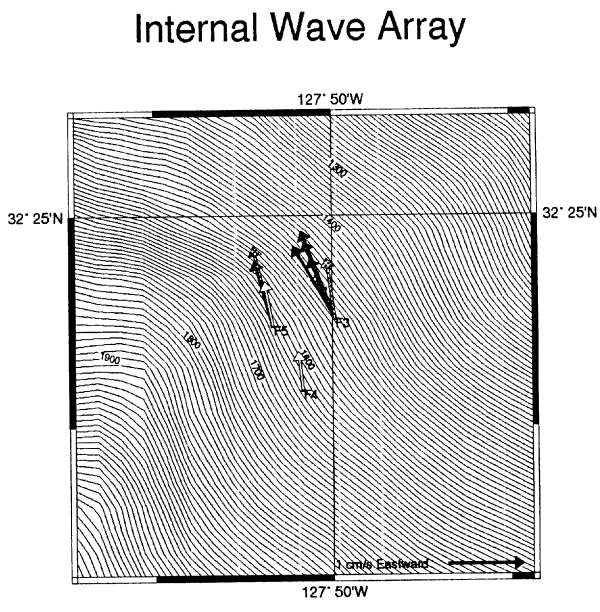

Figure 10. Mean flow over one year starting October 1, 1990, at 20 to 160 m above the bottom at the internal wave array sites. Currents 20 m from the bottom are drawn with a solid vector with currents farther off the bottom shaded more lightly to a height of 160 m, where vectors are unshaded. Instrument heights from the bottom are 20, 30, 40, 60, and 120 m off the bottom on F3, 160 m off the bottom on F4, and 40, 90, and 160 m off the bottom on F5. Depth contours at 10 m intervals are based on a Hydrosweep survey and the mooring position is based on acoustic and undithered GPS navigation. Surveyed depth exceeds that inferred from moored pressure records by 40-45 m at this site.

otherwise. Codiga, 1993, found subinertial oscillations to rectify into producing a low frequency anticyclonic swirl in a laboratory simulation.

The eddy fluxes in the vicinity of the summit plain rim are dominated by tidal, especially diurnal, fluctuations. The gradients in offslope buoyancy flux above the summit plain and the flank imply mean Eulerian downwelling of about 50 m/day and upwelling of 5 m/day, respectively, in the two regions according to the balance in (4), neglecting vertical mixing. Given the slope on the summit plain of about 0.05, about 1.2 cm/s of offslope flow is implied by mass conservation in the radial vertical plane, rather close to the flow observed (solid arrows, Figures 8 and 9) The linearized version of (2) relies on the vertical gradient of vertical eddy transport and radial gradient of radial transport of alongslope momentum to balance Coriolis acceleration. Referring to the two middle panels of Figure 7, both gradients appear of different sign at different locations. Since it is the sum of two terms, each of uncertain sign, that determines mean flow, no reliable estimate of radial flow can be made from this balance. The buoyancy flux structure, however, appears of the correct sign and magnitude to explain the offslope flow found near the bottom at the rim.

The eddy flux structure near the bottom on the flank also suggests an Eulerian mean flow of the sign observed, but due to internal wave rather than tidal processes. Radial buoyancy flux is in the offslope sense due to internal wave fluctuations (top left panel, Figure 4) and diminishes with distance from the bottom, whether offslope or vertical. The magnitude of vertical eddy buoyancy flux by wave breaking and the scale over which it changes implies that it can be neglected as a source of induced upwelling in the balance (4). The convergent pattern of radial buoyancy flux implies an upwelling of roughly 13 m/day. This, together with the bottom slope within the internal wave array of 0.45 implies an onslope flow of about 0.03 cm/s. This estimate is at least a factor of 3 weaker than what is observed directly. The linear version of the azimuthal momentum balance (2) on the flank is clearer than it is near the summit rim. The two flux gradient terms partially offset one another, but vertical gradients of vertical transport are somewhat larger than offslope

gradients of offslope transport of alongslope momentum. The difference implies an onslope mean flow of about 0.3 cm/s, a factor of 3 or so larger than what is measured directly. The mass and azimuthal momentum balances predict onslope flows that bracket that is observed directly, while neither balance agrees well with the current meter observations.

Trapped Waves over a Sloping Plane

The fluctuations observed at Fieberling Guyot span a relatively broad frequency range that includes the inertial frequency. While Brink, 1989, has found free resonant solutions trapped to a seamount, these are restricted to subinertial frequencies. Kunze, 1995, has suggested that the diurnal frequency fluctuations at Fieberling are dynamically superinertial waves confined to the anticyclonic vortex near the seamount summit. Although vortex trapped waves support a radial buoyancy flux and vertical phase propagation, both observed features, the observed waves extend to the bottom on the seamount flanks well beyond where the vortex is found and exist at superinertial frequencies where they could not be trapped by a vortex with only anticyclonic vorticity. Radial-vertical seamount trapped modes support neither radial buoyancy flux nor vertical phase propagation, but they do extend to the bottom. Brink, 1990, considered a forced problem, where the seamount response is a superposition of standing modes each excited off resonance, but the forcing was only at the diurnal (subinertial) frequency.

The purpose of this section is to point out that bottom-trapped waves can exist at both subinertial and superinertial frequencies that exhibit vertical phase propagation and support onslope heat flux, at least in infinite sloping plane geometry. Rhines, 1970, found the special case of these waves that satisfies no normal flow at the bottom and propagates freely both along and across isobaths, but always with shallow water to the right. Since motion is everywhere parallel to the bottom and rectilinear, these waves cannot support an onslope buoyancy flux. Propagating rays of this type at the same frequency can be combined to form vertical-onslope standing modes. Whether propagating or standing, these wave modes can be though of as a Kelvin wave generalized to continuous stratification over a sloping plane bottom. The more general form of these waves does not satisfy the simple slip boundary condition, hence these must be forced by normal flow at the boundary. They are evanescent waves. They do support onslope buoyancy flux, appear to propagate along the boundary, and can exist over a range of superinertial and at all subinertial frequencies. They are the response to periodic normal flow forced at the boundary.

The linear inviscid equations of motion in a uniformly stratified fluid over an infinite planar bottom can be written as:

$$u_t - fv = -p_x \tag{5a}$$

$$v_t + fu = -p_y \tag{5b}$$

$$N^2 w + w_{tt} = -p_{zt} \tag{5c}$$

$$u_x + v_y + w_z = 0 \tag{5d}$$

where (u,v,w) specifies the onslope, alongslope, and upward current components of flow in a right-handed coordinate system, p is reduced pressure, and N and f are the buoyancy frequency and Coriolis parameter. Propagating plane wave solutions that are trapped to a planar bottom with slope s specified by $z=sx$ exist when u,v,w and p all vary as $e^{i(kx+ly+mz-\sigma t)}e^{K(sx-z)}$ where (k,l,m) specify (real) wavenumber components and Ks and K are the (real) offslope and upward decay rates. (The decay scale normal to the boundary is $\left(K\sqrt{1+s^2}\right)^{-1}$ or $\frac{\cos\alpha}{K}$ where $s \equiv \tan\alpha$.) The system of equations (5) reduces to:

$$Q(p_{xx}+p_{yy}) = p_{zz} \tag{6}$$

where $Q \equiv \frac{N^2-\sigma^2}{\sigma^2-f^2}$. Evanescent solutions to (6) are possible because two wavenumber components (onslope and vertical) are complex, while the third (alongslope) is real. Such solutions describe waves trapped to the boundary when the dispersion relations

$$\left(\frac{Ks}{\kappa}\right)^2 = -Qs^2\left(\cos^2\varphi + \frac{\sin^2\varphi}{\left(1-Qs^2\right)}\right) \tag{7a}$$

and

$$\frac{m}{k} = -Qs \tag{7b}$$

are satisfied, where $\kappa \equiv \sqrt{k^2+l^2}$ is the horizontal wavenumber magnitude and the angle $\varphi \equiv Cos^{-1}\left(\frac{k}{\kappa}\right) = Sin^{-1}\left(\frac{l}{\kappa}\right) = Tan^{-1}\left(\frac{l}{k}\right)$ specifies the real wavenumber direction in the horizontal plane ($\varphi = 0$ is an onslope wave, $\varphi = \frac{\pi}{2}$ is an alongslope wave with shallow water on the right). For a given pressure signal p, the current components are:

$$u = \frac{\kappa p}{\sigma^2-f^2}\left(\sigma\cos\varphi + i\left(f\sin\varphi - \frac{\sigma Ks}{\kappa}\right)\right) \tag{8a}$$

$$v = \frac{\kappa p}{\sigma^2 - f^2}\left(\sigma \sin\varphi - \frac{fKs}{\kappa} - if\cos\varphi\right) \quad (8b)$$

$$w = \frac{\kappa p}{\sigma^2 - f^2}\left(\sigma s\cos\varphi - \frac{i\sigma K}{Q\kappa}\right). \quad (8c)$$

Solutions are valid for all direction angles φ for subinertial frequencies $\sigma < f$ but for only the restricted range of angles for which K remains real and positive in the range $f < \sigma < \sigma_c$, that is, at superinertial frequencies less than the internal wave critical frequency σ_c where $\sigma_c \equiv \sqrt{N^2 \sin^2\alpha + f^2 \cos^2\alpha}$. While these waves decay normal to the sloping bottom, phase lines are tilted upward and offslope at subinertial frequencies and upward and onslope at superinertial frequencies. They are level in the onslope-vertical plane at the inertial frequency. In the limit of vanishing frequency, phase lines attain an offslope-upward tilt of $\frac{f^2}{N^2 s}$. In the limit of the critical frequency, phase lines are parallel to the sloping bottom in the onslope-vertical plane.

The special case of these waves for which flow is everywhere parallel to the boundary, i.e., $w = su$, requires that:

$$\frac{Ks}{\kappa} = \frac{Qs^2 \frac{f}{\sigma}\sin\varphi}{Qs^2 - 1} \quad (9)$$

This restriction recovers the Rhines,1970, solution for edge waves. These are restricted to positive alongslope wavenumbers $l>0$ and to frequencies $\sigma < N\sin\alpha$, a more restrictive range than for evanescent waves.

The quantity $\frac{Ks}{\kappa}$ appearing in (7a) and (9) is the ratio of the horizontal length scale of the wave to its offslope decay scale. Large values of this ratio indicate that waves decay in only a fraction of a horizontal wave scale, thus are tightly bottom trapped. Contours of $\frac{Ks}{\kappa}$ calculated for parameters relevant to the summit region of Fieberling Guyot indicate that trapping is relatively gentle (i.e. $\frac{Ks}{\kappa} \sim 1$) for most wave orientations at superinertial frequencies and for orientations close to the alongslope direction at subinertial frequencies (Figure 11). While evanescent waves of any direction are possible at subinertial frequencies, the range of directions is tightly confined to alongslope at slightly superinertial frequencies, but broadens to nearly any direction close to the internal wave reflection critical frequency. Note that directions with an onslope component ($-\frac{\pi}{2} < \phi < \frac{\pi}{2}$) correspond to upward propagation at subinertial frequencies and downward propagation at superinertial frequencies and conversely for directions with an offslope component ($\frac{\pi}{2} < \varphi < \frac{3\pi}{2}$) by (7b) since Q changes sign (from $-\infty$ to $+\infty$) across the inertial frequency. Figure 11 is drawn only for the first two quadrants in direction because of these symmetries.

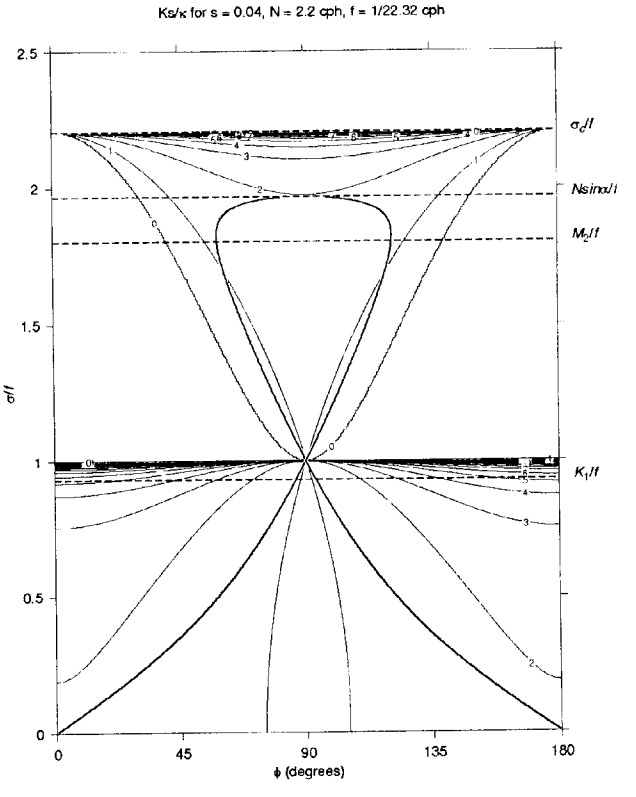

Figure 11. Ratio of horizontal length scale to offslope decay scale for evanescent waves as a function of frequency σ horizontal wavenumber vector orientation φ. Dispersion curves for edge waves are superimposed as heavy curves. Parameters are relevant to the summit region of Fieberling Guyot. Dashed lines mark the internal wave critical frequency (the maximum evanescent wave frequency), the maximum edge wave frequency, and the lunar semidiurnal and the lunisolar diurnal tidal frequencies. The ratio is not contoured where evanescent waves are not possible. Small ratios correspond to weak trapping. The orientations φ=0° and 90° correspond to pure onslope and alongslope (with shallow water to the right) propagation, respectively. Superinertial-onslope and subinertial-offslope waves propagate downward, and conversely.

Edge waves, however, are restricted to the range of directions plotted (all alongslope with shallow water to the right for $f>0$). These dispersion curves are drawn on the same set of axes as heavy curves in Figure 11. For the slope, stratification, and rotation parameters relevant to the summit region of Fieberling Guyot (s=0.04, N=2.2 cph, f=1/22.32 cph), edge waves are moderately trapped over their complete frequency range.

Both diurnal and semidiurnal tidal frequencies fall within the range of possible evanescent and edge wave frequencies (Figure 11). Diurnal frequency motions are only slightly subinertial and, as such, will be strongly trapped for all orientations except those nearly alongslope. Diurnal edge waves are aligned 3.6° onslope and offslope from the alongslope direction. At superinertial frequencies, the range of possible orientations broadens with increasing frequency. Semidiurnal edge waves attain nearly the most cross-isobath orientation possible over the possible range of superinertial frequencies. These and evanescent waves are weakly to at most moderately trapped to the bottom at superinertial frequencies (Note $0<\frac{Ks}{\kappa}<2$ for superinertial frequencies in this case).

Evanescent and edge wave amplitudes in pressure p can be expressed in terms of the energy density of the waves. The average energy per unit frequency per unit surface area normal to the slope E is

$$E = \frac{\rho_0 \kappa^2 \langle PP^* \rangle}{8K\left(\sigma^2 - f^2\right)^2}\left\{\left(\sigma^2 + f^2\right)\left(1 + \frac{K^2 s^2}{\kappa^2}\right)\right. \qquad (10)$$

$$\left. - 4\sigma f \frac{Ks}{\kappa}\sin\varphi + \left(\sigma^2 + N^2\right)\left(s^2 \cos^2\varphi + \frac{K^2}{Q^2 \kappa^2}\right)\right\}$$

where $\langle PP^* \rangle$ is the variance in reduced pressure per unit frequency at the bottom $z = sx$. The energy density E is a sum of potential and horizontal and vertical kinetic energies averaged over a wave period. Given the energy density E, the component amplitudes (u,v,w) appearing in (8) can be found by interpreting the amplitude of p as the standard deviation of pressure found in a specified frequency band from the spectrum $\langle PP^* \rangle$ since $\langle pp^* \rangle = \langle PP^* \rangle e^{2K(sx-z)}$. Normalization by energy density E allows currents associated with waves of different frequency or wavenumber to be compared, as with the current ellipses discussed next.

The current ellipse signature of evanescent waves varies considerably with wave orientation and frequency. The current ellipses in the horizontal and vertical-onslope planes for diurnal evanescent waves over a small range of wavenumber vector orientations (79.2°<φ<90°) that includes the edge wave orientation are given in Figure 12. Horizontal ellipses and horizontal projections of wavenumber vectors are given in the top row of this figure for waves directed onslope. Vertical-onslope current ellipses (with a vertical exaggeration of 10) are given in the second row. The lower two rows display the corresponding ellipses for waves with offslope senses. The sense of rotation of the current vectors changes in both the horizontal and onslope-vertical planes depending on whether waves are directed more or less onslope or offslope than the edge wave. In general, current ellipses in the vertical-onslope plane intersect the bottom, demonstrating the need for motions to be forced normal to the bottom in order to excite evanescent waves. Edge waves have flow everywhere parallel to the bottom, so can exist as free waves. The ellipses of Figure 12 indicate how minor departures from no normal flow at the bottom can induce substantial horizontal current fluctuations.

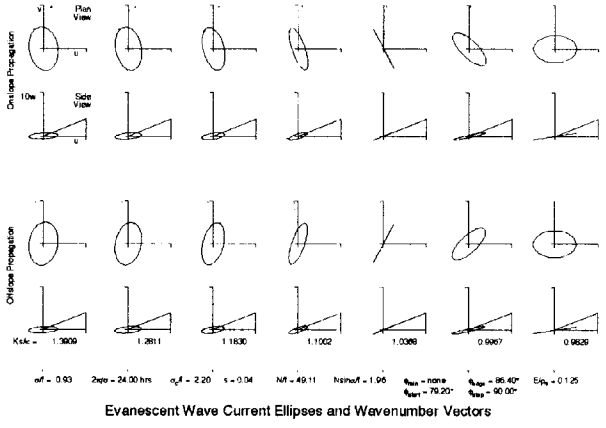

Figure 12. Current ellipses for evanescent waves of various orientation relative to isobaths at a fixed (diurnal) frequency. The top row shows current ellipses in the horizontal plane along with the horizontal projection of the wavenumber vector. The Second row shows corresponding current ellipses and the bottom slope in the onslope-vertical plane, exaggerated tenfold vertically. From right to left in each row, waves are directed more onslope and upward in the top two rows. The bottom two rows are the corresponding ellipses for waves directed increasingly offslope and downward from right to left. Waves are normalized to have equal energy.

Current ellipses for evanescent waves generally are not aligned with the wavenumber vector orientation. Waves travelling parallel to isobaths have current ellipses oriented normal to them, but in general horizontal ellipses and wavenumber vectors are not normal to one another. Edge waves not only have flow everywhere parallel to the bottom, but also have rectilinear flow

(ellipses collapse to straight lines). Pairs of rays with horizontal wavenumber vectors symmetric about the alongslope direction (i.e. $\varphi = \pm\frac{\pi}{2} \pm \theta$) can be summed to form standing modes in the vertical-onslope plane. In the case of standing modes, horizontal and vertical ellipses are oriented either parallel or normal to isobaths and the horizontal plane, respectively. Whereas individual rays can carry onslope or offslope momentum and buoyancy fluxes, standing modes cannot.

The horizontal buoyancy flux $F^b \equiv \langle u'b' \rangle$ of a propagating evanescent wave component is

$$F^b = -\frac{N^2 \langle pp^* \rangle \sigma K \kappa \cos\varphi}{2\left(\sigma^2 - f^2\right)^2} \left\{ \frac{f\kappa s}{\sigma K} \sin\varphi - s^2 + \frac{1}{Q} \right\} \quad (11)$$

The expression in curly brackets vanishes for edge waves, by (9). If the mean buoyancy balance is given by $WN^2 = -\frac{\partial}{\partial x} F^b$, (the rectilinear version of (4), but without vertical mixing), then the mean Eulerian upwelling induced by the waves is $W = -KsF^b N^{-2}$. By continuity, $U = W/s$. This Eulerian flow parallel to the bottom and decreasing exponentially from it with a scale $\cos\alpha\,(2K)^{-1}$, is exactly offset by the Stokes drift components $\left(U^S, W^S\right)$ which are equal and opposite to (U,W), in accordance with the predictions of nonacceleration theorems. So, while a mean Eulerian onslope or offslope flow can be induced by linear inviscid evanescent waves, there is no net Lagrangian circulation so induced. If mixing is introduced, the resulting non-zero Lagrangian mean circulation can be expected to have scales comparable to the domain in which the evanescent oscillations are found.

Discussion

The flow found near Fieberling Guyot is dominated by relatively narrow-band signals, and in this it is probably not unusual for a seamount. It is in strong contrast to open deep ocean flows, where mesoscale eddy motions tend to dominate current variance. The three strong characteristics of currents at Fieberling are 1) the mean anticyclone near the summit, 2) the diurnal-inertial-semidiurnal band of structurally similar flows, and 3) the near-critical reflection internal wave band. That fluctuations in the summit anticyclone modulate with the spring-neap cycle suggests that wave processes are important to its existence. Estimates of mean circulation in the vertical-radial plane based on eddy flux gradients, albeit crude, are in rough agreement with the horizontal currents measured directly. These suggest a pattern of downwelling above the summit plain and upwelling on the seamount flanks. There is no strong evidence that these flows are other than Eulerian means induced by the presence of bottom intensified wave motions. The level of mixing found by Eriksen, 1995, and the vertical scale over which it varies together are too small to produce mean flows even as big as the Eulerian flows observed.

Both internal wave band and diurnal motions effect measurable offslope buoyancy fluxes. Internal waves reflect off the steeply sloped flanks of the seamount in such a way as to generate rotary motions of current vectors in the vertical-onslope plane to generate offslope buoyancy flux near the bottom that decays with distance from it. Since these motions are strongest near the bottom, their decay implies a convergence of buoyancy flux, hence an induced (at least Eulerian) upwelling to compensate for it. The vertical gradients vertical buoyancy flux implied by the observed rate of density overturns are substantially weaker than observed horizontal gradients of offslope buoyancy flux.

Diurnal motions in the vertical onslope plane reach a maximum a hundred or more m above the seamount summit plain and at a finite radial distance from the seamount center, however roughly it can be defined. The offslope buoyancy flux these motions carry has gradients of both signs, implying downwelling at small radii (over the summit plain to about the rim) and upwelling outside this region, with the upwelling region more concentrated than that of downwelling. While there is considerable turbulent mixing reported above the summit plain, the magnitude of its gradients are weak compared to those of offslope buoyancy flux.

Neither the free seamount trapped wave whose resonant frequency is closest to the diurnal frequency (29 h period, according to Brink, 1995), nor the vortical trapped wave of Kunze, 1995, completely explains the nature of the diurnal and up-to-slightly-superinertial motions observed at Fieberling Guyot. The principal shortcomings of the seamount trapped wave model of Brink, 1990, are the failure to account for the observed phase propagation, offslope buoyancy flux, and frequency bandwidth (superinertial as well as subinertial) of the motions at Fieberling. The vortex-trapped wave model of Kunze, 1995, accounts for downward phase propagation and offslope buoyancy flux, but cannot account for these features at superinertial frequencies nor at depths and radii well removed from the near-summit intensified anticyclone.

An examination of uniformly stratified rotating flow over a planar sloping boundary demonstrates that, at least locally, evanescent and edge waves are possible at both subinertial and superinertial frequencies. These waves are bottom trapped with scales that can be comparable to

the degree of trapping observed at Fieberling. They can propagate vertically and horizontally with scales that are also comparable to those observed at Fieberling. The possibility of trapped wave motions at superinertial frequencies occurs because even though the governing equation (6) is hyperbolic for $\sigma > f$ ($Q > 0$), two complex wavenumber components can be offset by a real third component, hence waves can be trapped in two dimensions, and propagate in the third. These waves are possible in addition to free internal gravity waves (which propagate in all three dimensions). The possible generalization of this solution to arbitrary stratification and bottom boundary shape is not clear. Nevertheless, evanescent waves can be expected to be supported where stratification and bottom slope are locally uniform.

The response of a seamount to externally imposed flow is equivalent to forcing flow normal to the bottom at the bottom. The prominent responses found at Fieberling are at the diurnal and semidiurnal tides. The forced response of a linear, inviscid system can be calculated by the projection of forcing onto the normal modes of the system. This approach was followed by Brink, 1990, where the response away from resonance was calculated as the sum of phase-locked free modes. Seamount trapped waves form a complete discrete basis set and the projection of forcing at arbitrary frequencies defines the contribution of each mode to the total response. While individual modes are standing in the vertical-offslope plane, the phase-locked sum of such modes should lead to apparent vertical-radial phase propagation at arbitrary locations. Curiously, the Brink, 1995, solutions do not indicate sufficiently robust phase differences to match observed phase changes. Brink's normal modes are subinertial only so that if superinertial trapped free modes are possible, they may contribute to forced response as well.

The ray solutions of evanescent waves at a particular frequency can be summed over a variety of wavenumber orientations to produce a response that not only exhibits phase propagation, but varies the shape of current ellipses with distance from the bottom. Such a response could be formed by forcing with an arbitrary waveform at a particular frequency.

Acknowledgments

I thank Robert Reid, John Dahlen, and their colleagues at the C. S. Draper Laboratory, the captains and crews of R/V Washington and R/V Thompson, and Neil Bogue for help in carrying out the moored measurements. The analysis benefitted from discussions with Chris Garrett, Dan Codiga, Eric Kunze, and Ken Brink. This study was part of the U. S. Office of Naval Research Accelerated Research Initiative on Flow over Abrupt Topography and was supported under ONR grant numbers N00014-89-J-1621 and N00014-94-I-0081.

References

Brink, K. H., 1989: The effect of stratification on seamount-trapped waves, *Deep-Sea Res.*, 36, 825-844.

Brink, K. H., 1990: On the generation of seamount-trapped waves, *Deep-Sea Res.*, 37, 1569-1582.

Brink, K. H., 1995: Tidal and lower frequency currents above Fieberling Guyot, *J. Geophys. Res.*, 100, 10817-10832.

Chapman, D. C. and D. B. Haidvogel, 1992: Formation of Taylor caps over a tall isolated seamount in a stratified ocean, *Geophys. Astrophys. Fluid Dyn.*, 64, 31-65.

Codiga, D. L., 1993: Laboratory realizations of stratified seamount-trapped waves. *J. Phys. Oceanogr.*, 23, 2053-2071.

Eriksen, C. C., 1985: Moored observations of deep low-frequency motions in the central Pacific Ocean: Vertical structure and interpretation as equatorial waves, *J. Phys. Oceanogr.*, 15, 1085-1113.

Eriksen, C. C., 1991: Observations of amplified flows atop a large seamount, *J. Geophys. Res.*, 96, 15227-15236.

Eriksen, C. C., 1995: Internal wave reflection and mixing at Fieberling Guyot, *J. Geophys. Res.*, in press.

Kunze, E., and J. M. Toole, 1995: Fine- and microstructure observations of trapped diurnal oscillations atop Fieberling seamount, *Proceedings of the 1995 'Aha Huliko'a Hawaiian Winter Workshop*, this volume.

McIntyre, M. E., 1980: An introduction to the generalized Lagrangian-mean description of wave, mean-flow interaction, *Pure and Applied Geophys.*, 118, 152-176.

Rhines, P., 1970: Edge-, bottom-, and Rossby waves in a rotating stratified fluid, *Geophys. Fluid Dyn.*, 1, 273-302.

Roden, G. I., 1991: Mesoscale flow and thermohaline structure around Fieberling seamount, *J. Geophys. Res.*, 96, 16653-16672.

Roden, G. I., 1994: Effects of the Fieberling seamount group upon flow and thermohaline structure in the spring of 1991, *J. Geophys. Res.*, 99, 9941-9961.

Wallace, J. M., and R. F. Dickinson, 1972: Empirical orthogonal representation of time series in the frequency domain. Part I: Theoretical considerations, J. Appl. Meteor., 11, 887-892.

Wichman, C. A., C. C. Eriksen, N. M. Bogue, K. H. Brink, D. E. Frey, R. D. Pillsbury, G. M. Pittock, and S. A. Tarbell, 1993: Fieberling Guyot moored array data, *School of Oceanography Technical Report A93-1*, Univ. of Washington, Seattle, 373 pp.